

1 **Averaging over spatiotemporal heterogeneity substantially biases evapotranspiration rates in a mechanistic**
2 **large-scale land evaporation model**

3 Elham Rouholahnejad Freund^{1,2,3}, Massimiliano Zappa⁴, James W. Kirchner^{3,4,5}

4
5 ¹Laboratory of Hydrology and Water Management, Ghent University, Ghent, Belgium

6 ²Chair of Hydrology, Faculty of Environment and Natural Resources, University of Freiburg, Freiburg, Germany

7 ³Department of Environmental Systems Science, ETH Zurich, CH-8092 Zürich, Switzerland

8 ⁴Swiss Federal Research Institute WSL, CH-8903 Birmensdorf, Switzerland

9 ⁵Department of Earth and Planetary Science, University of California, Berkeley, CA 94720 USA

10

11 Correspondence to: Elham Rouholahnejad Freund, elham.rouholahnejad@gmail.com

12

13 **Abstract**

14 Evapotranspiration (ET) influences land-climate interactions, regulates the hydrological cycle, and contributes
15 to the Earth's energy balance. Due to its feedback to large-scale hydrological processes and its impact on
16 atmospheric dynamics, ET is one of the drivers of droughts and heatwaves. Existing land surface models differ
17 substantially, both in their estimates of current ET fluxes and in their projections of how ET will evolve in the
18 future. Any bias in estimated ET fluxes will affect the partitioning between sensible and latent heat, and thus
19 alter model predictions of temperature and precipitation. One potential source of bias is the so-called
20 "aggregation bias" that arises whenever nonlinear processes, such as those that regulate ET fluxes, are
21 modeled using averages of heterogeneous inputs. Here we demonstrate a general mathematical approach to
22 quantifying and correcting for this aggregation bias, using the GLEAM land evaporation model as a relatively
23 simple example. We demonstrate that this aggregation bias can lead to substantial overestimates in ET fluxes
24 in a typical large-scale land surface model when sub-grid heterogeneities in land surface properties are
25 averaged out. Using Switzerland as a test case, we examine the scale-dependence of this aggregation bias and
26 show that it can lead to an average overestimation of daily ET fluxes by as much as 10% across the whole
27 country (calculated as the median of the daily bias over the growing season). We show how our approach can
28 be used to identify the dominant drivers of aggregation bias, and to estimate sub-grid closure relationships
29 that can correct for aggregation biases in ET estimates, without explicitly representing sub-grid heterogeneities
30 in large-scale land surface models.

31 **Plain Language Summary**

32 Evapotranspiration (ET) is the largest flux from the land to the atmosphere and thus contributes to Earth's
33 energy and water balance. Due to its impact on atmospheric dynamics, ET is a key driver of droughts and
34 heatwaves. In this paper, we demonstrate how averaging over land surface heterogeneity contributes to
35 substantial overestimates of ET fluxes. We also demonstrate how one can correct for the effects of small-scale
36 heterogeneity without explicitly representing it in land surface models.

37

38 1. Introduction

39 Earth's surface and subsurface are characterized by spatial heterogeneity spanning wide ranges of scales,
40 including scales that cannot be explicitly resolved by large-scale Earth System Models (ESMs), which are
41 typically run at resolutions of 10-100 kilometers. Averaging over this finer-scale heterogeneity can bias model
42 estimates of water and energy fluxes and hence alter future temperature predictions. Earth system model
43 estimates of global terrestrial evaporation differ substantially from atmospheric reanalyses based on in-situ
44 and satellite remote sensing observations (Mueller et al., 2013), but it is unclear how much of these
45 differences could be attributed to errors in capturing sub-grid heterogeneity.

46

47 Several recent studies (e.g., Fan et al., 2019; Shrestha et al., 2018) have emphasized the need to account for
48 land surface heterogeneity in large-scale ESMs. Despite recent community efforts in refining ESMs' spatial
49 resolution (Huang et al., 2016; Rauscher et al., 2010; Ringler et al., 2008; Skamarock et al., 2012; Zarzycki et al.,
50 2014), the grid resolution of present-day ESMs is still too coarse to explicitly capture important effects of
51 surface heterogeneity. Whether the solution lies in hyper-resolution large-scale land surface modeling remains
52 an open question, because heterogeneities that are important to land-atmosphere fluxes will not be fully
53 resolved even at scales of 100 m (Beven and Cloke, 2012).

54

55 The effects of aggregating over spatial heterogeneity in land surface models have been assessed using several
56 approaches. Most of these approaches compare grid-cell-averaged energy and water fluxes with flux estimates
57 for finer-resolution grids, or for grid cells that are subdivided into mosaics of several surface types which
58 separately exchange momentum, energy, and water vapor with the overlying atmosphere (e.g., Giorgi, 1997).
59 Several studies have reported increases in average evapotranspiration (ET) (e.g., Kuo et al., 1999; Boone and
60 Wetzel, 1998; Hong et al., 2009; McCabe and Wood, 2006; El Maayar and Chen, 2006), and at least one has
61 reported decreases in grid-cell average ET (Ershadi et al., 2013), as model grids are coarsened and less spatial
62 heterogeneity is accounted for. Shrestha et al. (2018) studied the effects of horizontal grid resolution on ET
63 partitioning in the TerrSysMP Earth system model and found that the aggregation of topography decreases
64 average slope gradients and obscures small-scale convergence and divergence zones, directly impacting
65 surface and subsurface flow. They observed 5 and 8 percent decreases in the transpiration/evapotranspiration
66 ratio for a dry and a wet year, respectively, when their model grid cells were coarsened from 120 m to 960 m.
67 All these studies calculate the effects of land surface heterogeneity on ET fluxes using numerical experiments
68 that refine the model's spatial resolution, either directly or through the use of land-surface mosaics.

69

70 Quantifying the effect of sub-grid scale heterogeneity on grid-cell-averaged fluxes is especially important when
71 highly nonlinear processes are involved. Regardless of scale, the main challenge is not to explicitly represent
72 the heterogeneity in all its details, but instead to define an appropriate scale-dependent sub-grid closure
73 relationship that recognizes the important heterogeneities within the grid elements and the nonlinearities in

74 the processes (Beven, 2006). Such a sub-grid closure scheme would capture the effects of sub-grid
75 heterogeneity in large-scale land surface models without forcing them to run at finer spatial resolutions.
76

77 We have recently proposed a general theoretical framework, based on Taylor series expansions, that
78 quantifies the "aggregation bias" that results from averaging over sub-grid heterogeneity when grid-cell-
79 averaged ET is estimated (Rouholahnejad Freund and Kirchner, 2017; Rouholahnejad Freund et al., 2019). In
80 contrast to the numerical experiments described above, this theoretical framework does not depend on a
81 particular evapotranspiration model or grid scale. Our previous work demonstrated this framework using
82 Budyko curves as a see-through "toy" model, leaving open the question of how strongly ET estimates would be
83 affected by sub-grid heterogeneity in a more typical mechanistic evapotranspiration model. Here we use the
84 mechanistic evapotranspiration model GLEAM to quantify how aggregation biases vary across a range of
85 scales, using Switzerland as a case study. We show how our Taylor expansion framework can be used to
86 quantify the sensitivity of ET fluxes to heterogeneity in their individual drivers. We further demonstrate how
87 this framework can be used to estimate correction factors (i.e., sub-grid closure relationships) that account for
88 the effects of sub-grid heterogeneity without explicitly modeling it, and show how these correction factors can
89 be used to improve grid-scale ET estimates. Because our framework is not model-specific, the analysis
90 presented here could also be applied to many other evapotranspiration algorithms.

91

92 **2. Methods and results**

93 **2.1. A common mechanistic framework for predicting evapotranspiration**

94 Most large-scale land surface models calculate ET as a function of available water and energy at daily time
95 steps. They typically multiply an estimate of potential evapotranspiration (PET) by a conversion factor to
96 calculate actual evapotranspiration. PET is generally understood as the maximum rate of evapotranspiration
97 from a large area (to avoid the effect of local advection) covered completely and uniformly by actively growing
98 vegetation with adequate moisture at all times (Brutseart, 1984). Models typically estimate PET using the
99 Penman equation (Penman, 1948; intended for open water surfaces), the Penman-Monteith equation
100 (Monteith, 1965, Monteith and Unsworth, 1990; intended for reference crop evapotranspiration by adding
101 atmospheric transport processes and stomatal resistance to Penman's open water evaporation), or the
102 Priestley-Taylor equation (Priestley and Taylor, 1972; intended for open water and water-saturated crops and
103 grasslands). The conversion factor that is used to estimate ET from PET typically depends on plant physiology
104 and on the water that is available for evaporation.

105

106 Here, we employ an ET algorithm that is used by several land surface models (i.e., Global Land-surface
107 Evaporation: The Amsterdam Methodology (GLEAM); Miralles et al., 2011; Martens et al., 2017), in which
108 actual ET is calculated as a fraction of PET. This fraction is expressed as a multiplicative factor, often called a
109 stress factor, which ranges between 0 and 1 and thus limits ET rates. Under wet conditions, ET can equal PET
110 (stress factor equals one) while under dry conditions, PET is multiplied by a stress factor smaller than one
111 depending on the degree of water stress. This approach is employed by the GLEAM model, among others.

112 GLEAM is a diagnostic satellite-data-driven method that is used to estimate global land evaporation fluxes.
 113 GLEAM uses the Priestley-Taylor formula and remotely sensed datasets of radiation and temperature to
 114 calculate PET. In GLEAM, actual ET is calculated by constraining PET estimates by a stress factor that is based
 115 on estimates of root-zone soil moisture. The root zone soil moisture is derived from a multi-layer water
 116 balance module that describes the infiltration of precipitation through the vertical soil profile. ET estimates
 117 from GLEAM have been applied in many studies (e.g., Miralles et al., 2013; Miralles et al., 2014; Greve et al.,
 118 2014; Jasechko et al., 2013). GLEAM operates on daily time steps at 0.25-degree spatial resolution. To the best
 119 of our knowledge, there are no prior studies quantifying the aggregation bias in ET estimates from GLEAM or
 120 other models with similar ET formulations.

121

122 GLEAM calculates ET as an explicit function of the stress factor and potential evaporation:

$$123 \quad ET = S \cdot PET + (1 - \beta) I, \quad (1)$$

124 where ET is actual evapotranspiration (mm d^{-1}), S is the evaporative stress factor (-) that accounts for
 125 environmental conditions that reduce actual ET relative to potential ET, I is interception loss (mm d^{-1}), and β is
 126 a constant ($\beta = 0.07$ – Gash and Stewart, 1977) that avoids double-counting of interception losses during hours
 127 with wet canopy. The stress factor (S) depends on the soil moisture conditions, and is parametrized separately
 128 for tall canopy, short vegetation, and bare soil. GLEAM uses the following soil-moisture-based
 129 parameterization to calculate the stress factor (Miralles et al., 2011; Martens et al., 2017):

$$130 \quad S = 1 - \left(\frac{w_c - w_w}{w_c - w_{wp}} \right)^2, \quad (2)$$

131 where S is the stress factor (-) for tall canopy, w_w is the volumetric soil moisture at any given time ($\text{m}^3 \text{m}^{-3}$), and
 132 w_c and w_{wp} are the critical soil moisture level and soil moisture at wilting point. For soil moisture values below
 133 the wilting point w_{wp} , the stress is maximal (stress factor equals 0), causing ET to sharply decline to zero. For
 134 values above the critical moisture level w_c , there is no water stress (stress factor equals 1) and ET equals PET.
 135 Between w_{wp} and w_c the stress increases as soil moisture decreases following a parabolic function (Eq. 2). In
 136 the analysis presented below, we set the critical soil moisture level (w_c) and soil moisture at wilting point
 137 (w_{wp}) to 0.6 and 0.1 $\text{m}^3 \text{m}^{-3}$ respectively. To simplify the analysis presented below, we have used the tall-
 138 canopy stress factor (Eq. 2) for all of Switzerland, even though the short-canopy or bare-soil formulations may
 139 be better suited to some locations.

140

141 GLEAM uses the Priestley-Taylor approach to calculate PET (Priestley and Taylor, 1972):

$$142 \quad PET = \frac{\alpha}{\lambda} \frac{\Delta}{\Delta + \gamma} (R_n - G), \quad (3)$$

143 where PET is potential evapotranspiration (mm d^{-1}), α is a dimensionless coefficient that parametrizes the
 144 resistance to evaporation and is set to 0.8 for tall canopy in GLEAM (Miralles et al., 2011), $\lambda = 2.26$ (MJ kg^{-1}) is
 145 the latent heat of vaporization, R_n is net radiation ($\text{MJ m}^{-2} \text{d}^{-1}$), G is the ground heat flux, approximated as
 146 $G = 0.05 R_n$ ($\text{MJ m}^{-2} \text{d}^{-1}$) for tall canopy in GLEAM, T is temperature ($^{\circ}\text{C}$), and Δ is the slope of the

147 temperature/saturated vapor pressure curve ($\text{kPa}^\circ\text{C}^{-1}$), which is functionally related to temperature (Tetens,
148 1930; Murray, 1967; Stanghellini, 1987):

$$149 \quad \Delta = ae^{bT}, \quad (4)$$

150 where $a = 0.04145$ ($\text{kPa}^\circ\text{C}^{-1}$), $b = 0.06088$ ($^\circ\text{C}^{-1}$), and γ is the psychrometric constant ($\text{kPa}^\circ\text{C}^{-1}$) which can be
151 calculated as (Brunt, 1952):

$$152 \quad \gamma = \frac{C_{p_{air}} * P}{\lambda * MW_{ratio}}, \quad (5)$$

153 where $C_{p_{air}} = 0.001013$ ($\text{MJ kg}^{-1}\text{C}^{-1}$) is the specific heat of air at constant pressure, $P = 101.3$ (KPa) is
154 atmospheric pressure, and $MW_{ratio} = 0.622$ (-) is the molecular weight ratio of $\text{H}_2\text{O}/\text{air}$. Substituting the
155 aforementioned constants in Eq. 5 yields $\gamma = 0.073$ ($\text{kPa}^\circ\text{C}^{-1}$). Expanding Eq. 1 using Eqs. 2-5 yields the ET
156 function as calculated by GLEAM:

$$157 \quad \begin{aligned} ET_{[mmd^{-1}]} &= \left[-4w_w[m^3m^{-3}]^2 + 4.8w_w[m^3m^{-3}] - 0.44 \right] * \frac{\alpha_{[]}}{\lambda_{[MJ kg^{-1}]} * \Delta_{[kPa^\circ C^{-1}]} + \gamma_{[kPa^\circ C^{-1}]}} \\ &\quad * 0.95 * \frac{86400}{1000000} * R_n[w_m^{-2}] + (1 - \beta) I_{[mmd^{-1}]} \\ &= \left[-4w_w^2 + 4.8w_w - 0.44 \right] * 0.02905 * \frac{a e^{bT}}{a e^{bT} + 0.073} R_n + (1 - 0.07) I_{[mmd^{-1}]} \end{aligned} \quad (6)$$

158
159 In the analysis below, we use the GLEAM evapotranspiration algorithm to demonstrate how aggregation biases
160 can be estimated in land surface modeling schemes. We chose GLEAM because its governing equations are
161 amenable to the analytical solutions derived below. Here we make no particular claim for the accuracy or
162 validity of GLEAM as an evapotranspiration model, nor is our analysis intended to test this. Likewise our
163 analysis should not be interpreted as implying that GLEAM is any more, or less, susceptible to aggregation bias
164 than other evapotranspiration schemes, because this question is beyond the scope of the current paper.

165

166 **2.2. Mathematical framework for predicting aggregation bias**

167 *Nonlinear averaging using second-order Taylor expansions*

168 ET is a nonlinear function of its drivers. An intrinsic property of any nonlinear function is that the average of
169 the function will not equal the function evaluated at the average inputs (e.g., Rastetter et al., 1992; Giorgi and
170 Avissar, 1997; Rouholahnejad Freund and Kirchner, 2017). Thus averaging over sub-grid heterogeneity in ET
171 drivers, as large-scale land surface models do, would be expected to lead to biased ET estimates, even if the
172 underlying equations were exactly correct. For an ET function of three variables, namely R_n , w_w , and T , the
173 mean of the ET function, in terms of the function's value at the mean of its inputs, can be approximated by the
174 second-order Taylor series expansion of the ET function (Eq. 6):

$$175 \quad \begin{aligned} \overline{ET} &\approx \widehat{ET} + \frac{1}{2} \left[\frac{\partial^2 ET}{\partial R_n^2} \text{Var}(R_n) + \frac{\partial^2 ET}{\partial w_w^2} \text{Var}(w_w) + \frac{\partial^2 ET}{\partial T^2} \text{Var}(T) \right] \\ &\quad + \frac{\partial^2 ET}{\partial R_n \partial T} \text{Cov}(R_n, T) + \frac{\partial^2 ET}{\partial R_n \partial w_w} \text{Cov}(R_n, w_w) + \frac{\partial^2 ET}{\partial w_w \partial T} \text{Cov}(w_w, T), \end{aligned} \quad (7)$$

176 where \overline{ET} is the estimate of the true average of the nonlinear ET function over its variable inputs, \widehat{ET} is the ET
177 function evaluated at its mean inputs, and the derivatives are understood to be evaluated at the mean values
178 of the variables ($\overline{R_n}, \overline{w_w}, \overline{T}$) and multiplied by the corresponding variances and covariances among finer-

179 resolution input data. For the specific case of the GLEAM model, the ET function is evaluated at its mean inputs
 180 (\overline{ET}) and these derivatives are derived analytically from the ET function described by Eq. 6, directly yielding the
 181 following expressions:

$$182 \quad \widehat{ET} = [-4\overline{w}_w^2 + 4.8\overline{w}_w - 0.44] * 0.02905 * \frac{a e^{b\overline{T}}}{a e^{b\overline{T}} + 0.073} \overline{R}_n, \quad (8)$$

$$183 \quad \frac{\partial^2 ET}{\partial R_n^2} = 0, \quad (9)$$

$$184 \quad \frac{\partial^2 ET}{\partial w_w^2} = [-8] * 0.02905 * \frac{\Delta}{\Delta + \gamma} R_n \quad (w_{wp} \leq w_w \leq w_c), \quad (10a)$$

$$185 \quad \frac{\partial^2 ET}{\partial w_w^2} = 0 \quad (w_w < w_{wp}, \quad w_w > w_c), \quad (10b)$$

$$186 \quad \frac{\partial^2 ET}{\partial T^2} = [-4w_w^2 + 4.8w_w - 0.44] * 0.02905 * R_n * b^2 * \frac{\gamma^2 \Delta - \gamma \Delta^2}{(\gamma + \Delta)^3}, \quad (11)$$

$$187 \quad \frac{\partial^2 ET}{\partial R_n \partial T} = [-4w_w^2 + 4.8w_w - 0.44] * 0.02905 * \frac{\Delta}{\Delta + \gamma} * \frac{b\gamma}{\Delta + \gamma}, \quad (12)$$

$$188 \quad \frac{\partial^2 ET}{\partial R_n \partial w_w} = [-8w_w + 4.8] * 0.02905 * \frac{\Delta}{\Delta + \gamma} \quad (w_{wp} \leq w_w \leq w_c), \quad (13a)$$

$$189 \quad \frac{\partial^2 ET}{\partial R_n \partial w_w} = 0 \quad (w_w < w_{wp}, \quad w_w > w_c), \quad (13b)$$

$$190 \quad \frac{\partial^2 ET}{\partial w_w \partial T} = [-8w_w + 4.8] * 0.02905 * \frac{\Delta}{\Delta + \gamma} * \frac{b\gamma}{\Delta + \gamma} * R_n \quad (w_{wp} \leq w_w \leq w_c), \quad \text{and} \quad (14a)$$

$$191 \quad \frac{\partial^2 ET}{\partial w_w \partial T} = 0 \quad (w_w < w_{wp}, \quad w_w > w_c), \quad (14b)$$

192 where Δ depends on temperature as described in Eq. (4). The difference between the average of the functions
 193 (\overline{ET}) and the function of the averages (\widehat{ET}), or, equivalently, the sum of all the other terms in Eq. (7),
 194 represents the aggregation bias. The magnitude of this bias can be calculated by combining Eqs. 7-14 with
 195 estimates of the variances and covariances of the input variables. Note that the interception term in equation
 196 6 is dropped out from the derivatives as the interception loss in GLEAM is a linear function of amount of
 197 rainfall necessary to saturate the canopy and therefore has negligible effect when averaged.

198
 199 The approach outlined in Eq. (7) is general and could be extended to other land surface modeling schemes.
 200 The partial derivatives in Eqs. (8-14), of course, are specific to the GLEAM equations; for other models they
 201 would differ. More complex land surface model algorithms may not have such simple analytical derivatives; in
 202 that case, the derivatives can be evaluated numerically.

203

204 **2.3. Sub-grid heterogeneity and aggregation bias in ET estimates across Switzerland**

205 Drivers of ET (i.e., soil moisture, net radiation, and temperature) can be highly heterogeneous within the grid
 206 cells of typical ESMs. Soil moisture can show pronounced spatial variability, especially in areas where surface
 207 roughness, porosity, and permeability vary by orders of magnitude across a variety of length scales (Giorgi and
 208 Avissar, 1997). Temperature and incoming radiation vary significantly with season, elevation, altitude, and

209 albedo. Switzerland, for example, shows strong local variations in average annual temperature, soil moisture
210 content, net radiation, and albedo (Fig. 1; albedo values in Fig. S1).

211

212 We quantified how averaging over spatial (and temporal) heterogeneities of ET drivers affects estimated ET at
213 several grid scales across Switzerland, as an example case for which high-resolution data are available. Our
214 analysis is based on 500-m input data of temperature (interpolation of MeteoSwiss data after Viviroli et al.,
215 2009), net radiation (Viviroli et al., 2009), and soil moisture (simulations from the hydrological model PREVAH,
216 Brunner et al., 2019; Speich et al., 2015; Orth et al., 2015; Zappa et al., 2003) at daily time steps for the 2004
217 growing season. Although our soil moisture data are derived from model simulations whose accuracy is
218 difficult to assess due to the scarcity of real-world soil moisture measurements, for our purposes all that is
219 necessary is that the simulated values exhibit realistically complex spatial variability.

220

221 We used the GLEAM equations, as outlined in Sect. 2, to calculate ET for each day at the 500-m resolution of
222 these input data. We use these 500-m ET estimates as virtual "truth" for the purpose of our analysis, because
223 our goal is not to determine whether GLEAM estimates of ET are accurate (compared to direct measurements,
224 for example), but rather to quantify how spatial aggregation affects them.

225

226 To quantify how spatial aggregation affects model estimates of ET, we calculated ET over larger spatial scales
227 in two different ways. First, we averaged the 500-m ET estimates over 1/32, 1/16, 1/8, 0.25, 0.5, 0.75, 1, and 2-
228 degree grid cells across Switzerland, to represent the "true" average ET at those grid scales. Second, we
229 averaged the 500-m input data (of temperature, soil moisture, and net radiation) over the same grid cells, and
230 then used these grid-cell-averaged input data in the GLEAM equations to calculate the modeled coarse-
231 resolution ET at each grid scale. The deviation of the modeled coarse-resolution ET from the "true" average ET
232 measures the aggregation bias. Because this numerical experiment uses the same model equations, based on
233 the same underlying data, for the ET calculations at each spatial resolution, it isolates spatial aggregation as
234 the only possible cause of the difference between the "true" average ET (\overline{ET} in Eq. 7) and the coarse-resolution
235 modeled ET (\widehat{ET} in Eq. 7) at each grid scale.

236

237 Figure 2a shows that the ET aggregation bias varies considerably across Switzerland, and also varies
238 considerably with grid scale. The average aggregation bias is higher at coarser grid scales, averaging 10% at 2-
239 and 1-degree grid resolution across all of Switzerland (calculated as the median of the daily aggregation biases
240 over the growing season; Fig. 2a). Smaller grid scales typically exhibit smaller aggregation biases (averaging 4%
241 at 1/16-degree grid resolution across all of Switzerland calculated as the median of the daily aggregation
242 biases over the growing season) because they typically average over less spatial heterogeneity, but even at the
243 smallest grid scales, aggregation biases can locally reach 40% as indicated by the scatter plot in Fig. 3. These
244 figures are medians of the daily aggregation biases over the entire growing season of 2004; the aggregation
245 biases of two randomly selected days (May 31st and July 21st, 2004) at several spatial scales lead to much larger
246 overestimation of ET in parts of southern Switzerland (Figs. S2, S3).

247

248 Using our 500-m input data, we can test how well Eq. (7) estimates the difference between the "true" average
249 ET and the coarse-resolution modeled ET at each grid scale. We used Eqs. (8-14) to calculate the partial
250 derivatives of the GLEAM equations for each grid cell and time step, using the grid-cell averaged values of the
251 input data. We then multiplied these derivatives by the corresponding variances and covariances among the
252 500-m input data to obtain bias estimates via Eq. (15) for each grid cell and time step:

$$\begin{aligned} \text{Bias} = \widehat{\text{ET}} - \overline{\text{ET}} \approx & -\frac{1}{2} \left[\frac{\partial^2 \text{ET}}{\partial R_n^2} \text{Var}(R_n) + \frac{\partial^2 \text{ET}}{\partial w_w^2} \text{Var}(w_w) + \frac{\partial^2 \text{ET}}{\partial T^2} \text{Var}(T) \right] \\ & - \frac{\partial^2 \text{ET}}{\partial R_n \partial T} \text{Cov}(R_n, T) - \frac{\partial^2 \text{ET}}{\partial R_n \partial w_w} \text{Cov}(R_n, w_w) - \frac{\partial^2 \text{ET}}{\partial w_w \partial T} \text{Cov}(w_w, T), \end{aligned} \quad (15)$$

254 where $\overline{\text{ET}}$ is the true average ET at some grid resolution, $\widehat{\text{ET}}$ is the modeled coarse-resolution ET at the same
255 spatial scale, the right-hand side is the Taylor expansion estimate of the aggregation bias. We then compared
256 these estimated biases against the "true" aggregation biases (the difference between the "true" average ET
257 and the coarse-resolution modeled ET) in the numerical experiment described above. The true bias, in other
258 words, is $\widehat{\text{ET}} - \overline{\text{ET}}$ in Eq. (15), and the estimated bias is the Taylor approximation on the right-hand side.

259

260 Figure 2b shows that the aggregation bias estimated by Eq. (15) is generally similar, in both overall magnitude
261 and spatial distribution, to the "true" aggregation biases calculated by the numerical experiment. This
262 comparison is shown more explicitly in Fig. 3, in which the estimated aggregation bias is compared with the
263 "true" aggregation bias for each grid cell at each grid scale. Figures 2 and 3 show that Eq. (15) is generally a
264 good predictor of aggregation bias. Both the estimated aggregation biases (Fig. 2) and the "true" aggregation
265 biases are markedly higher in regions of greater topographic complexity (Fig. S4).

266

267 **2.4. Correcting for aggregation bias**

268 2.4.1. Identifying drivers of aggregation bias

269 The Taylor expansion in Eq. (15) not only allows one to quantify the aggregation bias; it also allows one to
270 quantify the relative importance of the three input variables (net radiation, soil moisture, and temperature) as
271 drivers of that bias. Each of the terms in Eq. (15) combines a variance or covariance that expresses how
272 variable the input data are, and a second derivative that expresses how sensitive the average ET is to that
273 variability. Each of these terms – a derivative multiplied by a variance or covariance – has the same units as ET,
274 and thus they can be directly compared to one another.

275

276 Table 1 shows each of the aggregation bias terms, calculated over all of Switzerland for the two randomly
277 chosen days mentioned in Sect. 2.3 (May 31st and July 21st, 2004). For these two example days, the aggregation
278 bias is clearly dominated by a single term, associated with the variance of soil moisture. The variance in net
279 radiation (R_n) creates no aggregation bias, because GLEAM ET is a linear function of R_n ; thus positive and
280 negative deviations from average R_n will increase and decrease ET by exactly offsetting amounts. Similarly, the
281 variance in temperature (T) also results in little aggregation bias, because GLEAM ET increases nearly linearly

282 with T across a wide range of temperature. The covariance terms similarly lead to little aggregation bias. By
283 contrast, the strong curvature in the quadratic dependence of ET on soil moisture (Eq. 6) implies that positive
284 and negative deviations from mean soil moisture will not have offsetting ET effects, and thus that spatial
285 heterogeneity in soil moisture can significantly alter average ET.

286

287 2.4.2. Correcting for aggregation bias using sub-grid closure relationships

288 The Taylor expansion framework in Eq. (7) can be used not only to diagnose aggregation bias, but also to
289 estimate sub-grid closure relationships that correct for the effects of small-scale heterogeneity. The variance
290 and covariance terms in Eq. (7) express how sub-grid heterogeneity affects average ET at the grid scale,
291 implying that these aggregation bias estimates could be used to improve grid-scale ET estimates, without
292 explicitly modeling ET at high resolutions. This approach could be particularly useful in land surface algorithms
293 that are part of coarser-resolution Earth system models; in such cases it may be much more efficient to
294 evaluate Eqs. 7-14 at the coarse grid resolution than to directly evaluate the underlying ET model, Eq. 6, at
295 high resolution. The Taylor expansion approach could also be attractive where we lack spatially explicit high-
296 resolution maps of the ET drivers, but where their variances and covariances can nonetheless be estimated
297 from other sources (such as from the variability of topography, mapped soil units, remote sensing data, etc.).

298

299 It is beyond our scope here to construct such variance and covariance estimates, but we can illustrate how
300 they could potentially be used. The solid red symbols in Fig. 4 show the relationships between "true" average
301 ET and modeled grid-cell-averaged ET, for each grid cell (and one example day, May 31st, 2004) at several
302 different grid scales. For comparison, the open grey symbols in Fig. 4 show average ET estimated by the Taylor
303 expansion approach of Eq. (7), which corrects for sub-grid heterogeneity effects using only grid-cell-averaged
304 estimates of the ET drivers and their small-scale variances and covariances.

305

306 The heterogeneity-corrected ET estimates shown by the open symbols in Fig. 4 cluster much closer to the 1:1
307 line than the modeled grid-cell-averaged ET values shown by the solid red symbols, suggesting that the Taylor
308 expansion approach may substantially improve estimates of grid-cell-averaged ET. Real-world results may be
309 less clear than those shown in Fig. 4, because the heterogeneity-corrected ET estimates (the open symbols in
310 Fig. 4) are calculated using exact values for the variances and covariances of the ET drivers within each grid
311 cell, and in real-world cases these variances and covariances will not be known precisely. Figure 4 nonetheless
312 demonstrates the potential value of knowing, or being able to estimate, those variances and covariances.
313 Efforts to determine those variances and covariances can be focused on the terms that matter the most, if one
314 can identify the main drivers of aggregation bias using the methods described in Sect. 2.2 above.

315

316

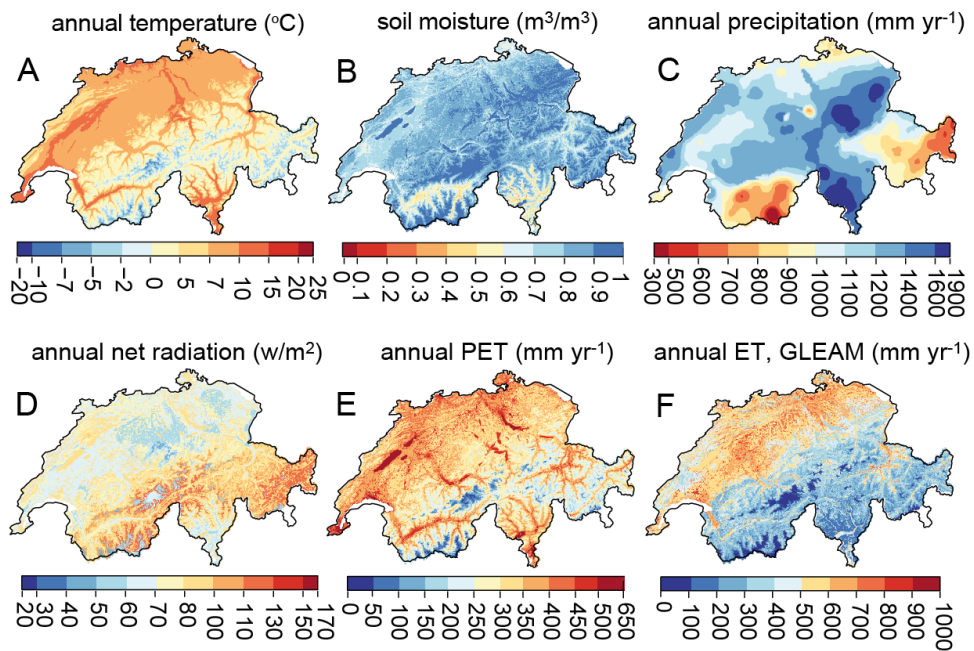
317
 318
 319
 320
 321
 322
 323
 324
 325
 326
 327

Table 1. Relative importance of different ET drivers in aggregation bias estimates (different terms in Eq. 15). Values are calculated for all of Switzerland for the two randomly chosen days (May 31st and July 21st, 2004). The aggregation bias is dominated by the term associated with the variance of soil moisture for these two example days.

	\widehat{ET} mm d ⁻¹	\overline{ET} mm d ⁻¹	Bias %	Contribution of $Var(R_n)$ term in % aggregation bias (%)	Contribution of $Var(w_w)$ term in % aggregation bias (%)	Contribution of $Var(T)$ term in % aggregation bias (%)	Contribution of $Cov(R_n, T)$ term in % aggregation bias (%)	Contribution of $Cov(R_n, w_w)$ term in % aggregation bias (%)	Contribution of $Cov(R_n, w_w)$ term in % aggregation bias (%)
Calculation	(Eq. 8)	(Eq. 7)	(Eq. 15)	$\frac{1}{2} \frac{\partial^2 ET}{\partial R_n^2} Var(R_n)$ ($\widehat{ET} \cdot Bias$)	$\frac{1}{2} \frac{\partial^2 ET}{\partial w_w^2} Var(w_w)$ ($\widehat{ET} \cdot Bias$)	$\frac{1}{2} \frac{\partial^2 ET}{\partial T^2} Var(T)$ ($\widehat{ET} \cdot Bias$)	$\frac{\partial^2 ET}{\partial R_n \partial T} Cov(R_n, T)$ ($\widehat{ET} \cdot Bias$)	$\frac{\partial^2 ET}{\partial R_n \partial w_w} Cov(R_n, w_w)$ ($\widehat{ET} \cdot Bias$)	$\frac{\partial^2 ET}{\partial w_w \partial T} Cov(w_w, T)$ ($\widehat{ET} \cdot Bias$)
31.05.2004	2.3	1.89	21.7	0	81.65	0.90	1.05	2.80	14.41
21.07.2004	2.11	1.84	14.84	0	83.35	2.34	6.56	1.84	6.01

328
 329

330
331



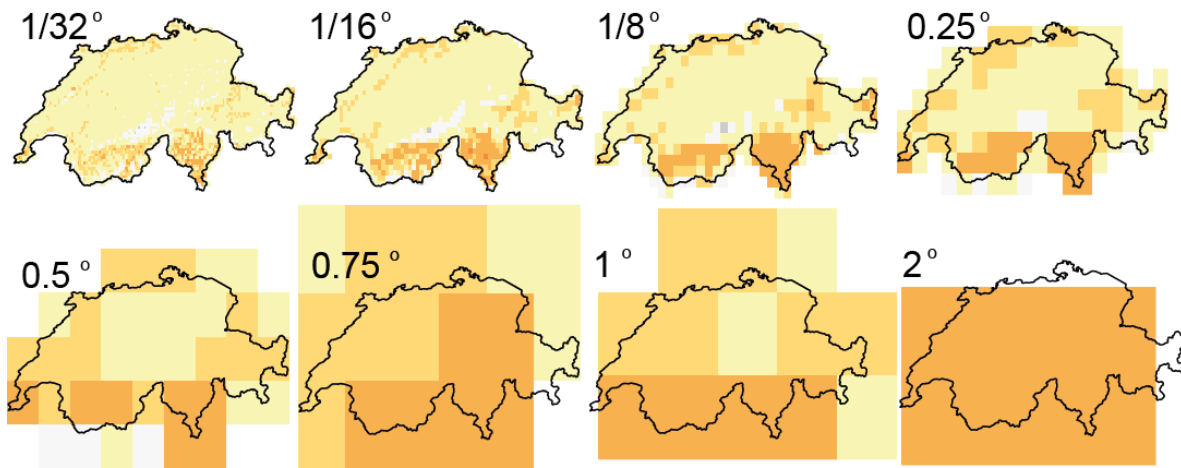
332

333 Figure 1. Spatial distribution of input data for the year 2004 at 500-m resolution: Annual mean (A) temperature
334 (°C), (B) soil moisture ($\text{m}^3 \text{m}^{-3}$, simulated by the PREVAH hydrological model), (C) precipitation (mm yr^{-1}), (D)
335 net radiation (W m^{-2}), (E) potential evapotranspiration (PET, mm yr^{-1}) using the Priestley-Taylor equation (Eq.
336 3), and (F) evapotranspiration (ET, mm yr^{-1}) using the approach used in the GLEAM model (Eq. 1). See Table. S1
337 for references.

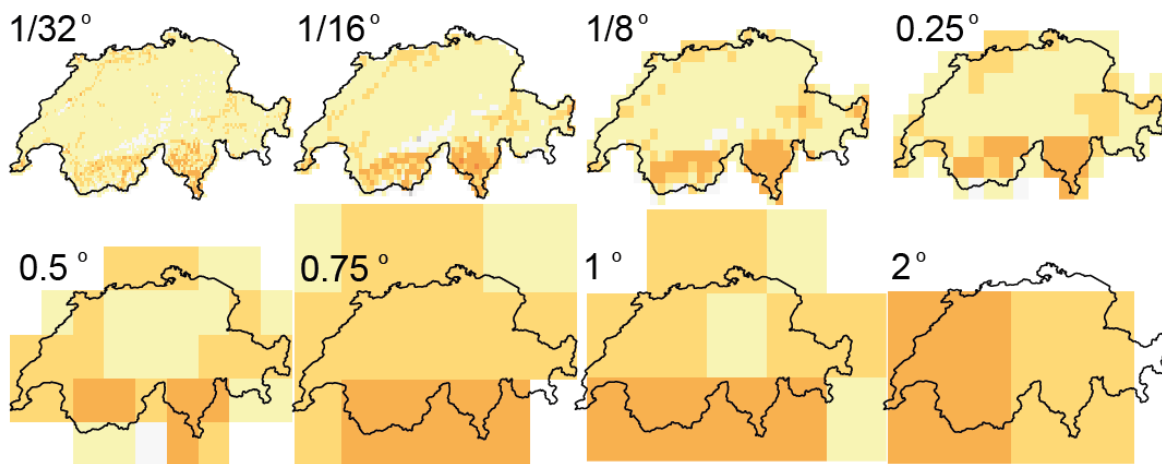
338

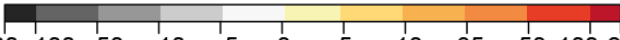
339

a) True Aggregation Bias (%)



b) Estimated Aggregation Bias (%)



340  % aggregation bias in ET estimate
 341 (median of daily errors in April-Oct 2004)

340

341 Figure 2. a) “True” aggregation bias in ET, as calculated by averaging the 500-m resolution ET estimates using

342 fine-resolution input data in Eq. 6, over 1/32, 1/16, 1/8, 0.25, 0.5, 0.75, 1, and 2-degree grid cells across

343 Switzerland. b) Aggregation bias in ET, as estimated by Eq. 7 from grid-cell averaged temperature ($^{\circ}\text{C}$), soil

344 moisture (w_w), net radiation (R_n), their variances at each grid scale, and the covariances of all pairs of variables

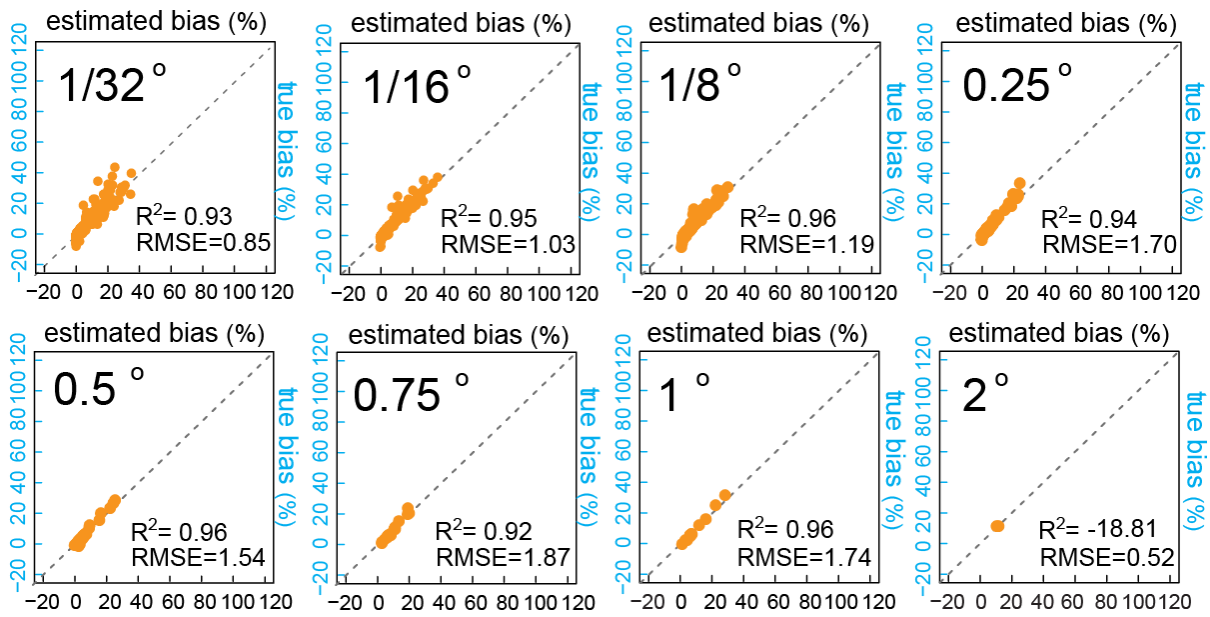
345 using the 500-m input data. At finer grid scales, the aggregation bias is more localized, and smaller on average.

346 Across Switzerland as a whole, average aggregation bias becomes smaller as grid scales become finer, but

347 never disappears completely.

348

349

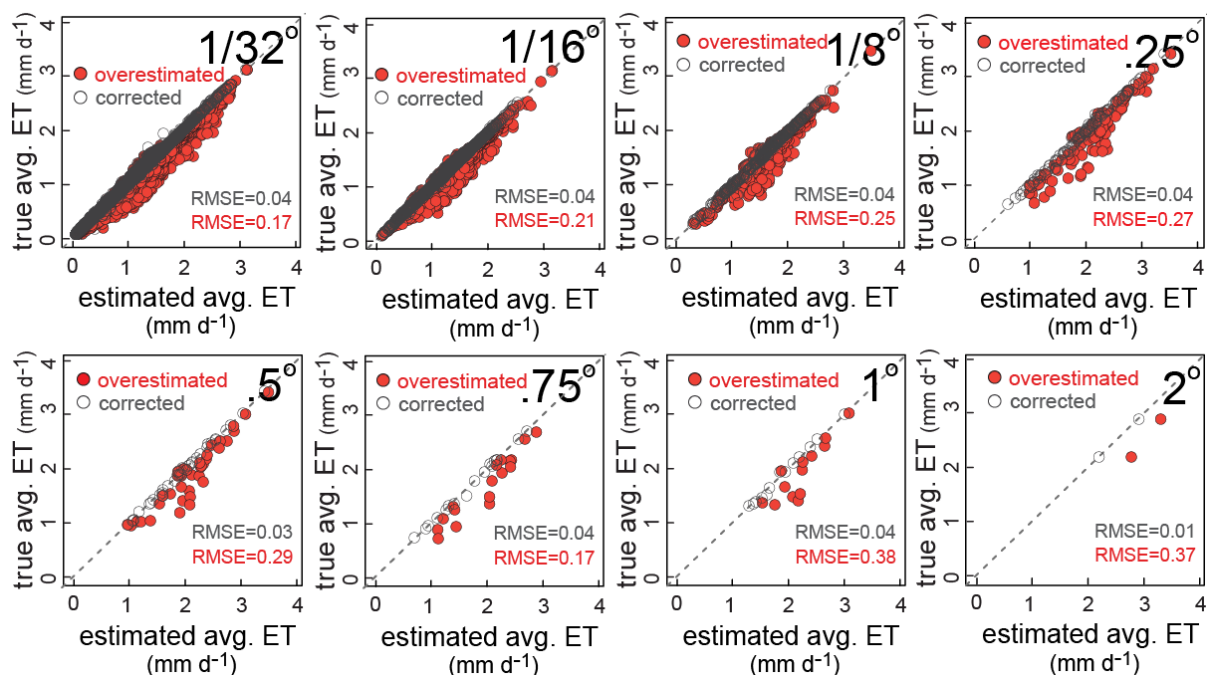


350

351 Figure 3. Daily estimated aggregation bias in ET estimates (% , median of daily biases in Apr.-Oct. 2004) versus
 352 daily true aggregation bias in ET estimates (% , median of daily biases in Apr.-Oct. 2004) at several spatial
 353 scales. Estimated aggregation biases are calculated using Eq. 7. True aggregation biases are calculated as
 354 differences between the finer resolution ET estimates from finer resolution input data, averaged over several
 355 spatial scales (average of functions) and ET values calculated from average inputs at each spatial scale
 356 (function of averages). The coefficients of determination (R^2) between the true and estimated aggregation
 357 biases verify the reliability of the Taylor expansion method and Eq. 7 as estimates of the aggregation bias.

358

359



361

362 Figure 4. Daily estimated ET rates versus “true” average ET at each grid cell at several different grid scales
 363 (example day, May 31st, 2004). The solid red symbols demonstrate the relationships between “true” average
 364 ET calculated using fine-resolution data at each grid cell and modeled grid-cell-averaged ET using grid-cell-
 365 averaged inputs in Eq.8, for each grid cell at several different grid scales (overestimated). For comparison, the
 366 open symbols show true average versus average ET estimated by the Taylor expansion approach of Eq. (7),
 367 which corrects for sub-grid heterogeneity effects using only grid-cell-averaged estimates of the ET drivers and
 368 their small-scale variances and covariances (heterogeneity-corrected ET estimates, corrected).

369

370 3. Discussion

371 Averaging over spatially heterogeneous ET drivers leads to substantial aggregation biases in ET flux estimates
 372 from a typical mechanistic large-scale land surface model. This aggregation bias arises from the inherent
 373 nonlinearities in evapotranspiration processes, coupled with the inherent spatial heterogeneity in the driving
 374 factors. The joint effects of these nonlinearities and heterogeneities can be estimated using second-order
 375 Taylor expansions of the governing equations. Using Switzerland as a test case, we have shown that median
 376 aggregation biases of 10-35% are common, even at grid scales substantially smaller than those typically used in
 377 land surface models (Fig. 2). These biases can be much larger for individual days (Figs. S2 and S3) and
 378 potentially have substantial consequences for water and energy flux estimates in land surface models and
 379 consequently for temperature predictions in coupled models. The overestimated evaporative fluxes would
 380 lead to overestimated latent heat fluxes and underestimated sensible heat fluxes, and thus potentially to
 381 underestimates of expected temperature increases in a changing climate. Unrealistically high evaporation
 382 estimates lead to cooler modeled temperatures and wetter modeled climates. Correcting for the aggregation

383 bias in ET fluxes would lead to reduced evaporative cooling and increased atmospheric heating via sensible
384 heat flux.

385

386 In coupled Earth system models, ET fluxes influence how surface temperature, net radiation, and soil moisture
387 evolve through time, and thus influence future values of ET. The analyses shown in Figs. 2-4 are based on static
388 values for each day, and thus do not account for the propagation of aggregation biases forward through time.
389 Estimating the consequences of aggregation biases for dynamic modeling would require fully coupled Earth
390 system model simulations rather than the single ET algorithm analyzed here. In a dynamic model, the Taylor
391 expansion approach can potentially be used to correct for aggregation biases in each time step, using
392 statistical models for the variances and covariances of the ET drivers. Thus, estimating aggregation biases in a
393 dynamic model would not require explicitly simulating sub-grid heterogeneity at every time step. Correcting
394 for aggregation biases at each modeling time step would prevent them from propagating further into future
395 time steps, or into the partitioning of future water and energy fluxes at the land surface. The present paper
396 does not illustrate this dynamic correction for aggregation biases, but establishes the theoretical framework
397 for it.

398

399 The purpose of our analysis was to demonstrate how aggregation bias due to spatial heterogeneity can be
400 quantified (Sects. 2.2-2.3), how its dominant drivers can be identified (Sect. 2.4.1), and how its effects can be
401 efficiently corrected for, using sub-grid closure relationships (Sect. 2.4.2). For this demonstration, we chose
402 GLEAM as an illustrative example, and Switzerland as a topographically complex case study where high-
403 resolution data on the ET drivers are available. Applications of this approach to more complex land surface
404 models may require calculating the necessary derivatives (see Eq. 7) numerically rather than analytically, and
405 applications where high-resolution data are unavailable may require statistically estimating the variances and
406 covariances among the drivers of ET, based on their relationships with topography, soil types, land cover, etc.
407 Using the approach outlined here, one can account for the effects of sub-grid heterogeneity without explicitly
408 modeling ET at fine spatial resolution, which could be impractical due to computational costs, or impossible
409 due to a lack of fine-resolution input data.

410

411 In our analysis, spatial heterogeneity in soil moisture emerged as the dominant driver of aggregation bias in ET
412 estimates. Particularly if this result can also be confirmed in other regions and climates, it points to the
413 importance of improving our understanding of spatial patterns of soil moisture and what controls them. The
414 lower topographic curvature of coarsely gridded landscapes can lead models to predict higher soil moisture at
415 coarser grid scales (Kuo et al., 1999); higher soil moisture at larger grid scales would lead to even higher
416 modeled values of ET, beyond the effects of the aggregation biases analyzed here. Soil moisture may also be
417 substantially influenced by lateral subsurface transfers of water, which are ignored in our analysis and are also

418 ignored by many land surface models. Overlooking lateral transfers could potentially bias ET estimates in large-
419 scale land surface models (Fan et al., 2019), but this is beyond the scope of the present study.

420

421

422 **Acknowledgements**

423 We thank Prof. Ying Fan Reinfelder for numerous insightful discussions and for helpful comments on the
424 manuscript. E.R.F. acknowledges support from the Swiss National Science Foundation (SNSF) under Grant No.
425 P2EZP2_162279.

426 **Data Availability Statement**

427 We will upload the source data for this study to a FAIR repository and provide the URL with the final version of
428 the paper.

429

430

431 **References**

- 432 Beven, K. J., and H. L. Cloke: Comment on “Hyperresolution global land surface modeling: Meeting a grand
433 challenge for monitoring Earth's terrestrial water” by Eric F. Wood et al., *Water Resour. Res.*, 48, W01801,
434 <https://doi.org/10.1029/2011WR010982>, 2012.
- 435 Beven, K. J.: The holy grail of scientific hydrology: $Q_t=H(SR)A$ as closure, *Hydrol. Earth Syst. Sci.*, 10, 609–618,
436 <https://doi.org/10.5194/hess-10-609-2006>, 2006.
- 437 Boone, A., and O. J. Wetzel: A simple scheme for modeling sub-grid soil texture variability for use in an
438 atmospheric climate model, *Journal of the Meteorological Society of Japan*, 77(1), 317–333,
439 https://doi.org/10.2151/jmsj1965.77.1B_317, 1998.
- 440 Brunner, M. I., K. Liechti, and M. Zappa: Extremeness of recent drought events in Switzerland: dependence on
441 variable and return period choice, *Natural Hazards and Earth System Science*, 19(10), 2311–2323,
442 <https://doi.org/10.5194/nhess-19-2311-2019>, 2019.
- 443 Brunt, D.: *Physical and dynamical meteorology*, 2nd ed., Univ. Press, Cambridge. 428 pp, 1952.
- 444 Brutsaert, W.: *Evaporation into the atmosphere*, ISBN 978-90-481-8365-4, [https://doi.org/10.1007/978-94-](https://doi.org/10.1007/978-94-017-1497-6)
445 [017-1497-6](https://doi.org/10.1007/978-94-017-1497-6), 1984.
- 446 BFS, *Die Bodennutzung der Schweiz: Arealstatistik 1979/85*, Bundesamt fuer Statistik, Bern, 1995.
- 447 Budyko, M. I.: *Climate and life*, Academic, New York, 1974.
- 448 Bundesamt für Landestopographie: *Digitales Höhenmodell RIMINI*, Wabern,
449 [https://www.bfs.admin.ch/bfs/de/home/dienstleistungen/geostat/geodaten-](https://www.bfs.admin.ch/bfs/de/home/dienstleistungen/geostat/geodaten-bundesstatistik/topografie.assetdetail.230215.html)
450 [bundesstatistik/topografie.assetdetail.230215.html](https://www.bfs.admin.ch/bfs/de/home/dienstleistungen/geostat/geodaten-bundesstatistik/topografie.assetdetail.230215.html), 1991.
- 451 El Maayar, M. , and J. M. Chen: Spatial scaling of evapotranspiration as affected by heterogeneities in
452 vegetation, topography, and soil texture, *Remote Sensing of Environment*, 102, 33–51,
453 <https://doi.org/10.1016/j.rse.2006.01.017>, 2006.
- 454 Ershadi A., M. F. McCabe, J. P. Evans, and J. P. Walker: Effects of spatial aggregation on the multi-scale
455 estimation of evapotranspiration, *Remote Sensing of Environment*, 131, 51–62,
456 <http://dx.doi.org/10.1016/j.rse.2012.12.007>, 2013.
- 457 Fan, Y., M. Clark, D. M. Lawrence, S. Swenson, L. E. Band, S. L. Brantley, P. D. Brooks, W. E. Dietrich, A. Flores,
458 G. Grant, J. W. Kirchner, D. S. Mackay, J. J. McDonnell, P. C. D. Milly, P. L. Sullivan, C. Tague, H. Ajami, N.
459 Chaney, A. Hartmann, P. Hazenberg, J. McNamara, J. Pelletier, J. Perket, E. Rouholahnejad-Freund, T. Wagener,
460 X. Zeng, E. Beighley, J. Buzan, M. Huang, B. Livneh, B. P. Mohanty, B. Nijssen, M. Safeeq, C. Shen, W. van
461 Verseveld, and J. Volk, D. Yamazaki: Hillslope hydrology in global change research and Earth system modeling,
462 *Water Resources Research*, 55, <https://doi.org/10.1029/2018WR023903>, 2019.
- 463 Gash, J. H. C.: an analytical model of rainfall interception by forests, *Q. J. R. Meteorol. Soc.* 105 (433), 43–55,
464 <https://doi.org/10.1002/qj.49710544304>, 1979.

465 Giorgi, F.: An Approach for the Representation of Surface Heterogeneity in Land Surface Models. Part I:
466 Theoretical Framework, *Mon. Wea. Rev.*, 125, 1885–1899, [https://doi.org/10.1175/1520-](https://doi.org/10.1175/1520-0493(1997)125<1885:AAFTRO>2.0.CO;2)
467 [0493\(1997\)125<1885:AAFTRO>2.0.CO;2](https://doi.org/10.1175/1520-0493(1997)125<1885:AAFTRO>2.0.CO;2), 1997.

468 Giorgi, F., and R. Avissar: Representation of heterogeneity effects in Earth system modeling: Experience from
469 land surface modeling, *Rev. Geophys.*, 35, 413–437, <https://doi.org/10.1029/97RG01754>, 1997.

470 Greve, P., B. Orlowsky, B. Mueller, J. Sheffield, M. Reichstein, and S. I. Seneviratne: Global assessment of
471 trends in wetting and drying over land, *Nature Geoscience*, 7: 716, 2014.

472 Hong, S. H., J. M. H. Hendrickx, and B. Borchers: Up-scaling of SEBAL derived evapotranspiration maps from
473 Landsat (30 m) to MODIS (250 m) scale, *Journal of Hydrology*, 370, 122–138,
474 <https://doi.org/10.1016/j.jhydrol.2009.03.002>, 2009.

475 Huang, X., A. M. Rhoades, P. A. Ullrich, and C. M. Zarzycki: An evaluation of the variable-resolution- CESM for
476 modeling California’s climate, *J. Adv. Model. Earth Syst.*, 8, 345–369, doi:10.1002/2015MS000559, 2016.

477 Jasechko, S., Z. D. Sharp, J. J. Gibson, S. J. Birks, Y. Yi, and P. J. Fawcett: Terrestrial water fluxes dominated by
478 transpiration, *Nature*, 496: 347, <https://doi.org/10.1890/ES13-00391.1>, 2013.

479 Kuo, W. L., T. S. Steenhuis, C. E. McCulloch, C. L. Mohler, D. A. Weinstein, S. D. DeGloria, and D. P. Swaney:
480 Effect of grid size on runoff and soil moisture for a variable-source-area hydrology model, *Water Resour. Res.*,
481 35(11), 3419–3428, <https://doi.org/10.1029/1999WR900183>, 1999.

482 Martens, B., D. G. Miralles, H. Lievens, R. van der Schalie, R. A. M. de Jeu, D. Fernández-Prieto, H. E. Beck, W. A.
483 Dorigo, and N. E. C. Verhoest: GLEAM v3: satellite-based land evaporation and root-zone soil moisture, *Geosci.*
484 *Model Dev.* 10(5): 1903–1925, <https://doi.org/10.5194/gmd-10-1903-2017>, 2017.

485 McCabe M., and E. Wood: Scale influences on the remote estimation of evapotranspiration using multiple
486 satellite sensors, *Remote Sensing of Environment* 105, 271–285, <https://doi.org/10.1016/j.rse.2006.07.006>,
487 2006.

488 Miralles, D. G., T. R. H. Holmes, R. A. M. De Jeu, J. H. Gash, A. G. C. A. Meesters, and A. J. Dolman: Global land-
489 surface evaporation estimated from satellite-based observations, *Hydrol. Earth Syst. Sci.* 15(2): 453–469,
490 <https://doi.org/10.5194/hess-15-453-2011>, 2011.

491 Miralles, D. G., A. J. Teuling, C. C. van Heerwaarden, and J. Vilà-Guerau de Arellano: Mega-heatwave
492 temperatures due to combined soil desiccation and atmospheric heat accumulation, *Nature Geosci.* 7(5):
493 345–349, <https://doi.org/10.1038/NGEO2141>, 2014.

494 Miralles, D. G., M. J. van den Berg, J. H. Gash, R. M. Parinussa, R. A. M. de Jeu, H. E. Beck, T. R. H. Holmes, C.
495 Jiménez, N. E. C. Verhoest, W. A. Dorigo, A. J. Teuling, and A. Johannes Dolman: El Niño–La Niña cycle and
496 recent trends in continental evaporation, *Nature Climate Change*, 4: 122,
497 <https://doi.org/10.1038/NCLIMATE2068>, 2013.

498 Monteith, J. L., and M. H. Unsworth: *Principles of Environmental Physics*, Edward Arnold, London, 1990.

499 Monteith, J. L.: Evaporation and environment, the state of and movement of water in living organisms,
500 Proceeding of Soc. for Exp. Biol., 19, 205–234, doi:10.1002/qj.49710745102, 1965.

501 Mueller, B., M. Hirschi, C. Jimenez, P. Ciais, P. A. Dirmeyer, A. J. Dolman, J. B. Fisher, M. Jung, F. Ludwig, F.
502 Maignan, D. G. Miralles, M. F. McCabe, M. Reichstein, J. Sheffield, K. Wang, E. F. Wood, Y. Zhang, and S. I.
503 Seneviratne: Benchmark products for land evapotranspiration: LandFlux-EVAL multi-data set synthesis, *Hydrol.*
504 *Earth Syst. Sci.* 17(10): 3707–3720, <https://doi.org/10.5194/hess-17-3707-2013>, 2013.

505 Murray, F. W.: On the computation of saturation vapor pressure, *J. Appl. Meteor.* 6: 203–204,
506 [https://doi.org/10.1175/1520-0450\(1967\)006<0203:OTCOSV>2.0.CO;2](https://doi.org/10.1175/1520-0450(1967)006<0203:OTCOSV>2.0.CO;2), 1967.

507 Orth, R., M. Staudinger, S. I. Seneviratne, J. Seibert, and M. Zappa: Does model performance improve with
508 complexity? A case study with three hydrological models, *Journal of Hydrology*, 523, 147–159,
509 <https://doi.org/10.1016/j.jhydrol.2015.01.044>, 2015.

510 Penman, H. L.: Natural evaporation from open water, bare soil, and grass, *Proc. Roy. Soc. London A*193,
511 120–146, 1948.

512 Priestley, C. H. B., and R. J. Taylor: On the assessment of surface heat flux and evaporation using large-scale
513 parameters, *Monthly Weather Review*, 100, 81–92, [https://doi.org/10.1175/1520-0493\(1972\)100<0081:otaosh>2.3.co;2](https://doi.org/10.1175/1520-0493(1972)100<0081:otaosh>2.3.co;2), 1972.

515 Rauscher, S. A., E. Coppola, C. Piani, and F. Giorgi: Resolution effects on regional climate model simulations of
516 seasonal precipitation over Europe, *Clim. Dyn.*, 35(4), 685–711, <https://doi.org/10.1007/s00382-009-0607-7>,
517 2010.

518 Ringler, T., L. Ju, and M. Gunzburger: A multiresolution method for climate system modeling: Application of
519 spherical centroidal Voronoi tessellations, *Ocean Dyn.*, 58(5–6), 475–498, <https://doi.org/10.1007/s10236-008-0157-2>, 2008.

521 Rouholahnejad Freund, E., and J. W. Kirchner: A Budyko framework for estimating how spatial heterogeneity
522 and lateral moisture redistribution affect average evapotranspiration rates as seen from the atmosphere,
523 *Hydrology and Earth System Sciences*, 21(1), 217–233, <https://doi.org/10.5194/hess-21-217-2017>, 2017.

524 Rouholahnejad Freund, E., Y. Fan, and J. W. Kirchner: Global assessment of how averaging over spatial
525 heterogeneity in precipitation and potential evapotranspiration affects modeled evapotranspiration rates,
526 *Hydrol. Earth Syst. Sci.*, 24, 1927–1938, <https://doi.org/10.5194/hess-24-1927-2020>, 2020.

527 Seneviratne, S. I., T. Corti, E. L. Davin, M. Hirschi, E. B. Jaeger, I. Lehner, B., Orlowsky, and A. J. Teuling:
528 Investigating soil moisture–climate interactions in a changing climate: A review, *Earth-Science Reviews* 99(3–
529 4): 125–161, <https://doi.org/10.1016/j.earscirev.2010.02.004>, 2010.

530 Shrestha, P., M. Sulis, C. Simmer, and S. Kollet: Impacts of grid resolution on surface energy fluxes simulated
531 with an integrated surface-groundwater flow model, *Hydrol. Earth Syst. Sci.* 19(10): 4317–4326,
532 <https://doi.org/10.5194/hess-19-4317-2015>, 2015.

533 Shrestha, P., M. Sulis, C. Simmer, and S. Kollet: Effects of horizontal grid resolution on evapotranspiration
534 partitioning using TerrSysMP, *Journal of Hydrology*, 557: 910–915,
535 <https://doi.org/10.1016/j.jhydrol.2018.01.024>, 2018.

536 Skamarock, W. C., J. B. Klemp, M. G. Duda, L. D. Fowler, S.-H. Park, and T. D. Ringler, A multiscale
537 nonhydrostatic atmospheric model using centroidal Voronoi tessellations and C-grid staggering, *Mon. Weather*
538 *Rev.*, 140(9), 3090–3105, <https://doi.org/10.1175/MWR-D-11-00215.1>, 2012.

539 Speich, M. J. R., L. Bernhard, A. J. Teuling, and M. Zappa: Application of bivariate mapping for hydrological
540 classification and analysis of temporal change and scale effects in Switzerland, *Journal of Hydrology*, 523, 804–
541 821, <https://doi.org/10.1016/j.jhydrol.2015.01.086>, 2015.

542 Stanghellini, C., *Transpiration of Greenhouse Crops*. PhD thesis, Wageningen University, Wageningen, The
543 Netherlands, 1987.

544 Tetens, O., Über einige meteorologische Begriffe. *z. Geophys.* 6:297–309, 1930.

545 Viviroli, D., M. Zappa, J. Gurtz, and R. Weingartner: An introduction to the hydrological modelling system
546 PREVAH and its pre- and post-processing-tools, *Environmental Modelling and Software*, 24(10), 1209–1222,
547 <https://doi.org/10.1016/j.envsoft.2009.04.001>, 2009.

548 Zappa, M. and J. Gurtz: Simulation of soil moisture and evapotranspiration in a soil profile during the 1999
549 MAP-Riviera Campaign, *Hydrol. Earth Syst. Sci.*, 7, 903–919, <https://doi.org/10.5194/hess-7-903-2003>, 2003.

550 Zarzycki, C. M., M. N. Levy, C. Jablonowski, J. R. Overfelt, M. A. Taylor, and P. A. Ullrich: Aquaplanet
551 experiments using CAM’s variable-resolution dynamical core, *J. Clim.*, 27(14), 5481–5503,
552 <https://doi.org/10.1175/JCLI-D-14-00004.1>, 2014.

553

554